Aggregation−Fragmentation in a Model of DNA-Mediated Colloidal Assembly

F. Pierce,* C. M. Sorensen, and A. Chakrabarti

Department of Physics, Kansas State University, Manhattan, Kansas 66506

Received March 14, 2005. In Final Form: August 4, 2005

We present results from an off-lattice Monte Carlo simulation of DNA-mediated colloidal assembly. In this simulation, the aggregation−fragmentation of a binary mixture of DNA-coated colloidal particles is studied through a simplified model of base-pair hybridization. Bonding between monomers is modeled as a simple temperature-sensitive A/B-type interaction, where type A and B monomers can bond to only the opposite type (no A/A or B/B attachments are allowed). The actual chemistry of base-pair hybridization is not included in the model. The morphological structures of the clusters formed as well as the kinetics of growth are analyzed in our 2D simulations. The fractal dimension and kinetic growth exponents for clusters formed near the DNA "melting" temperature agree with those seen previously for 2D diffusion-limited cluster aggregation (DLCA) models. The clusters appear more compact, exhibiting signs of local order at intermediate temperature values. At higher temperatures, the formation of large clusters is not favorable under the action of temperature-dependent fragmentation, and the system eventually reaches a steady state as a collection of small aggregates. The temperature profile for this *dissolution* of the colloidal assembly is sharp, indicating that the selective hybridization process provides a highly sensitive measurement tool. At high temperatures, we analyze the steady-state behavior of the average cluster size in terms of an aggregation−fragmentation model.

I. Introduction

Recent effort[1,2] has been directed toward the assembly of micrometer- or nanometer-sized colloidal particles into complex ordered structures by manipulating the strength and range of interaction between them. Tailoring of interactions among colloidal particles can be achieved in several ways. It is possible to control nonspecific interactions[3] (such as van der Waals or electrostatic forces) by changing the bulk material properties of suspensions. If the magnitude of the nonspecific interaction potential between colloidal particles is comparable to the thermal energy kT, then both rearrangement and fragmentation (hence reversible aggregation) of clusters can take place. For a charge-stabilized colloidal solution, this can happen with the addition of a salt or surfactant solution of predetermined molarity so that a secondary minimum (of a few k_BT depth) in the interaction potential forms.[4] Another way to control the interaction energy between colloidal particles is to induce a depletion interaction by adding a nonadsorbing polymer[5−7] or a differently sized colloid.[8] By varying the concentration and the length of the polymer chains, one can change the strength and range of the depletion interaction.

Recent advances in synthetic chemistry have given rise to a wide variety of nanoparticles with a high degree of both chemical and physical uniformity.[9−12] These nanoparticles are surface ligated with a variety of organic compounds and hence can form stable colloids in organic solvents. Also in many cases the precipitating solid is a 2D or 3D superlattice of the nanoparticles.[13,14] For ligated nanoparticle assembly, the interaction between two nanoparticles is a combination of van der Waals attractions and the steric repulsion between the tethered chains on the particles' surfaces.[15] By changing the ligand chain length and the composition of the particles and the solvent, one can again control the strength and range of the nonspecific interaction.

To control the assembly of colloidal and nanoparticles in a totally different yet effective way, several groups[16−21] have introduced specific biomolecular cross-linking among particles by coating these particles with complimentary biological complexes. Often these complexes are proteins or DNA molecules that behave as a specific lock and key and mediate attractive interaction only between specific colloidal particles. A selective aggregation is induced by coating species A and B with single-stranded DNA molecules (ssDNA) along with the addition of target ssDNA

(1) For a review, see Poon, W. C. K.; Haw, M. D. *Adv. Colloid Interface Sci.* **1997**, *73*, 71−126.
(2) For a review, see Anderson, V. J.; Lekkerkerker, H. N. W. *Nature* **2002**, *416*, 811−815.
(3) Russel, W. B.; Saville, D. A.; Schowalter, W. R. *Colloidal Dispersions*; Cambridge University Press: Cambridge, U.K., 1989.
(4) Israelachvili, J. *Intermolecular and Surface Forces*; Academic Press: San Diego, CA, 1994.
(5) Asakura, S.; Oosawa, F. *J. Chem. Phys.* **1954**, *22*, 1255−1256.
(6) Vrij, A. *Pure Appl. Chem.* **1976**, *48*, 471−473.
(7) Verma, R.; Crocker, J. C.; Lubensky, T. C.; Yodh, A. G. *Macromolecules* **2000**, *33*, 177−186.
(8) Hobbie, E. K. *Phys. Rev. Lett.* **1998**, *81*, 3996−3999.
(9) Klabunde, K. J. *Nanoscale Materials in Chemistry*; Wiley-Interscience: New York, 2001.
(10) Collier, C. P.; Vossmeyer, T.; Heath, J. R. *Annu. Rev. Mater. Sci.* **1998**, *49*, 371−404.
(11) Murray, C. B.; Kagan, C. R.; Bawendi, M. G. *Annu. Rev. Mater. Sci.* **2000**, *30*, 545−610.
(12) Lin, X. M.; Parthasarathy, R.; Jaeger, H. *Encyclopedia of Nanoscience and Nanotechnology*; Marcel Dekker: New York, 2004; pp 2245−2258.
(13) Murray, C. B.; Kagan, C. R.; Bawendi, M. G. *Science* **1995**, *270*, 1335−1338.
(14) Bentzon, M. D.; Wonterghem, J. V.; Morup, S.; Tholen, A. *Philos. Mag.* **1989**, *60*, 169−178.
(15) Raghavan, S. N.; Hou, J.; Baker, G. L.; Khan, S. A. *Langmuir* **2000**, *16*, 1066−1077.
(16) (a) Jin, R.; Wu, G.; Mirkin, C. A.; Schatz, G. C. *J. Am. Chem. Soc.* **2003**, *125*, 1643−1654. (b) Taton, T. A.; Mirkin, C. A.; Letsinger, R. L. *Science* **2000**, *289*, 1757−1760. (c) Mirkin, C. A.; Letsinger, R. L.; Mucic, R. C.; Storhoff, J. J. *Nature* **1996**, *382*, 607−609.
(17) Milam, V. T.; Hiddesen, A. L.; Crocker, J. C.; Graves, D. J.; Hammer, D. A. *Langmuir* **2003**, *19*, 10317−10323.
(18) Hiddesen, A. L.; Rodgers, S. D.; Weitz, D. A.; Hammer, D. A. *Langmuir* **2000**, *16*, 9744−9753.
(19) Cobbe, S.; Connolly, S.; Ryan, D.; Nagle, L.; Eritja, R.; Fitzmaurice, D. *J. Phys. Chem. B* **2003**, *107*, 470−477.
(20) Kisak, E. T.; Kennedy, M. T.; Trommeshauser, D.; Zasadzinski, J. A. *Langmuir* **2000**, *16*, 2825−2831.
(21) Seeman, N. C. *Nature* **2003**, *421*, 427−431.

10.1021/la050688z CCC: $30.25
Published on Web 08/27/2005

that can form links only between a pair of A and B type colloidal particles. The association between hybridized DNA strands is reversible upon heating above a "melting" temperature T_m. On one hand, the DNA-driven assembly of nanoparticles can be used as building blocks of complex materials synthesis, and on the other, the assembly can be used to detect mutations in a specific DNA sequence. For both of these applications, one needs to understand quantitatively how the dissolution of the DNA-driven assembly depends on the size of the particles and on the surface density and interaction strength (which might be controlled by changing the dielectric properties of the surrounding medium) of the DNA molecules. The morphology of the assembly as a function of this large set of variables is extremely important to understanding how to control the material properties (such as optical and electronic properties of the gold nanoparticle assembly). Moreover, if the dissolution of the assembly is very sharp, one can possibly map DNA sequences on the macroscopic phase behavior of the nanoparticle assembly.

There is a wealth of experimental data on the dissolution of DNA-linked nanoparticle assemblies. For example, Jin et al.[16] have analyzed the dependence of the dissolution temperature on the size of the particles and on the surface density and interaction strength of the DNA molecules. As the DNA coverage is increased, one obtains a higher dissolution temperature. Below the dissolution temperature the particles aggregate into a gellike state, whereas even slightly above the dissolution temperature the gel comes apart to form much smaller clusters. The sharpness of the dissolution temperature strongly indicates that multiple DNA linkers are formed between each pair of particles. A mean-field model introduced by Lukatsky and Frenkel[22] reproduces the experimental observation of a sharp dissolution temperature. However, this mean-field model completely ignores cluster morphology and thus cannot provide a detailed description of the assembly or the dissolution process.

As a first step toward providing a detailed theoretical understanding of the morphology and dissolution of DNA-mediated colloidal assemblies, we have carried out computer simulations of reversible aggregation of a binary mixture of colloidal particles through a simple model of base-pair hybridization between complementary DNA strands attached to the particles. Bonding between monomers is modeled as a simple temperature-sensitive A/B-type interaction, where type A and B monomers can bond to only the opposite type (no A/A or B/B attachments are allowed). The actual chemistry of base-pair hybridization is not included in the model. The morphological structures of the clusters formed as well as the kinetics of growth are analyzed in our 2D simulations. The parameters varied in this work include the coverage of DNA molecules on the particles, the number of possible DNA linkers between pairs of particles, the temperature, and the overall area fraction of colloidal particles. The fractal dimension and kinetic growth exponents for clusters formed near the melting temperature agree with those seen previously for 2D diffusion-limited cluster aggregation (DLCA) models.[23] At intermediate temperatures, the clusters appear more compact, exhibiting signs of local order. At higher temperatures, the formation of large clusters is not favorable under the action of temperature-dependent fragmentation, and the system eventually reaches a steady state consisting of a collection of small aggregates. In all cases studied, the temperature profiles are sharp, indicating that the selective hybridization process provides a highly sensitive measurement tool. The kinetics curves obtained from simulations are comparable to those of DLCA in the case of lower temperatures, whereas for intermediate temperatures, a complicated behavior is observed and a possible explanation based on coordination number and local order is offered. Steady-state behavior of the average cluster size at higher temperatures is analyzed in terms of a mean-field aggregation−fragmentation model.[24,25]

II. Model and Numerical Procedure

We model the experimental situation where species A and B are coated with single-stranded DNA molecules (ssDNA) and the addition of target ssDNA can form links only between a pair of A and B type colloidal particles. The temperature-dependent free-energy difference $\epsilon(T)$ of a double-stranded DNA molecule connecting a pair of A and B type colloidal particles is considered to have the form $\epsilon(T) = sk_B(T - T_m)$ following Lukatsky and Frenkel,[22] where T_m is the melting temperature of the target DNA, k_B is the Boltzmann constant, and $s = 10$. This expression represents the first term in the expansion of the exact free energy.[26] The choice of $s = 10$ in Lukatsky and Frenkel's model originates from the work of Rouzina and Bloomfield,[26] who report that the entropy difference between the two states of a DNA molecule is 25 cal/mol K (or $12.5k_B$), which is modeled by Lukatsky and Frenkel as $\sim 10k_B$. This is translated into the probability of forming a bond between a pair of A and B type colloidal particles as $p = \exp[-\epsilon(T)/k_BT]$, whereas the probability of a previously formed bond being severed is $1 - p$. When $T = T_m$, the interaction is irreversible ($p = 1$), but as T is increased, the fragmentation of clusters can take place.

To study the formation of DNA-mediated assembly of colloidal particles, we use an off-lattice Monte Carlo algorithm. Initially, 10 000 unbonded particles (monomers) of each type (A and B with complementary DNA strands) are placed at random in a square box with periodic boundary conditions. Our simulations are carried out in 2D because of computer time limitations, not because we want to model particle−substrate interactions. We have considered several monomer area fractions (f_a) ranging from $f_a = 0.01$ to 0.40. Clusters (initially monomers) are selected one at a time at random from the list of remaining clusters and moved a distance based on their diffusion constant, which is inversely proportional to their radius of gyration. The largest movement allowed for any cluster is one monomer diameter, corresponding to a cluster size of unity. After N_c (number of clusters left at the time) such moves, the Monte Carlo time is incremented by one unit, and a test is made for all system particles to determine what changes in bonding with neighbors have occurred. Particles of type A are allowed only to bind to particles of type B. To bind, the surfaces of the two particles must lie within a certain cutoff distance (in our case 0.1 times the monomer diameter). As mentioned before, a bond formed at some time t is allowed to break at a later time with probability $1 - p$. For each simulation, the total number of bonds for each particle (b_t) is set equal to a fixed value, as well as the maximum number of bonds between any two neighboring particles (b_n). Variations in

(22) Lukatsky, D. B.; Frenkel, D. *Phys. Rev. Lett.* **2004**, *92*, 068302.
(23) Meakin, P.; Vicsek, T.; Family, F. *Phys. Rev. B* **1985**, *31*, 564−569. Fry, D. Aggregation in Dense Particulate Systems. Ph.D. Thesis, Kansas State University, Manhattan, KS, 2003.
(24) Family, F.; Meakin, P.; Deutch, J. M. *Phys. Rev. Lett.* **1986**, *57*, 727−730.
(25) Sorensen, C. M.; Zhang, H. X.; Taylor, T. W. *Phys. Rev. Lett.* **1987**, *59*, 363−366.
(26) Rouzina, I.; Bloomfield, V. A. *Biophys. J.* **1999**, *77*, 3242−3251.

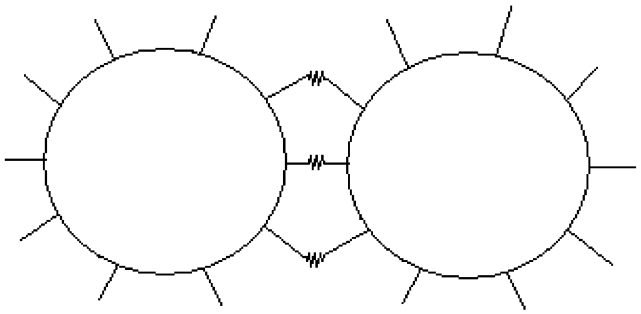

Figure 1. Sketch showing the possible bonding between two monomers in a simulation with $b_t = 10$, $b_n = 3$. DNA linkers are assumed to be distributed approximately symmetrically over the surface of the monomers, limiting the number of possible linker contacts between monomers.

the values of b_n and b_t approximately correspond to a variation of DNA coverage in an experimental situation and the presence of multiple DNA linkers between each pair of nanoparticles also observed in experiments.[16] For example, in the case of $b_t = 10$ and $b_n = 3$, a specific particle may make up to 10 bonds with neighboring particles of the opposite type, with up to 3 of those bonds with a particular neighbor (Figure 1). At $T = T_m$, only aggregation can take place because bond breaking is not possible. When $T > T_m$, the formation and severing of bonds between particles can take place, and evolution of the system is controlled by an aggregation kernel as well as a fragmentation kernel.

III. Results

A. Morphology of Growing Clusters. In Figure 2, we show snapshots of the structures formed for temperatures $T = 1.00$, 1.02, 1.04, and 1.05, respectively, in units of T_m. These images were taken at a late time in each simulation, where late time refers to the time at which the cluster number has reached a plateau. In each case, the monomer area fraction is $f_a = 0.10$ with $b_t = 10$ and $b_n = 3$. Cluster formation at the melting temperature ($T = T_m$) is irreversible, and the fractal morphology of the system is quite similar to DLCA aggregates in two dimensions (2D). The binary nature of the interactions between particles does not seem to alter the overall structure of the aggregates.[27] As shown in Figure 3a, the fractal dimension of these clusters rises from a value of ~1.40 to over 1.50. At later times, many collisions between clusters do not lead to an A−B binding, hence aggregates do not form in every collision. It is possible then that the binary colloid system may cross over from a DLCA morphology at early times to a reaction-limited (RLCA) morphology at late times.[27,28] The signature of this is present in the fractal dimension of the clusters that slowly increases from the lower value of 1.4, passes through 1.45 (the accepted 2d DLCA value), and approaches the 2D RLCA value[29] of 1.55.

As the temperature is increased from T_m, the fragmentation (and reaggregation) of clusters becomes possible, and as a result, the aggregation process becomes reversible. At a temperature of $T = 1.02T_m$, for example, we begin to notice the onset of compaction of the clusters. Visual inspection of cluster morphology at various times suggests that this compaction arises from a sequence

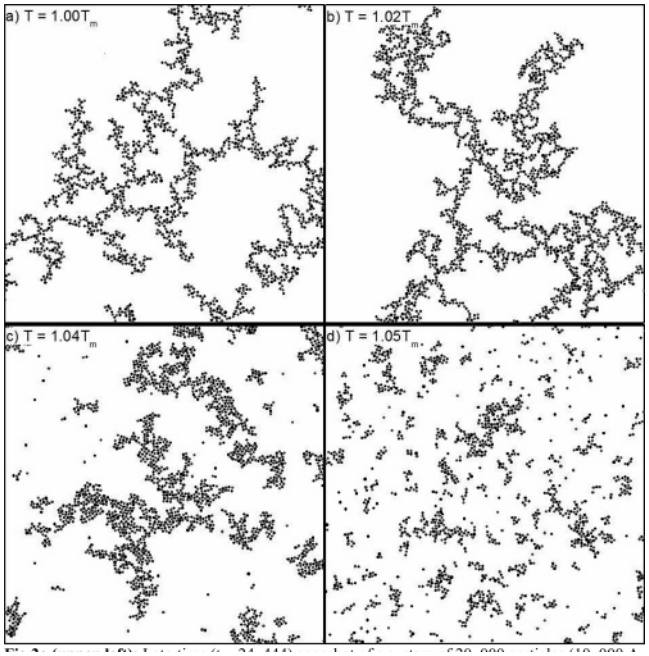

Figure 2. (a) Late-time ($t = 24\,444$) snapshot of a system of 20 000 particles (10 000 type A and 10 000 type B) at the DNA melting temperature T_m. At this temperature, only aggregation events occur, and gellike morphology is observed. Here $b_t = 10$, $b_n = 3$, and $f_a = 0.1$. (b) Same as in part a except $T = 1.02T_m$ and $t = 98\,349$. In comparison to the aggregation-only morphologies seen at T_m, the clusters here begin to exhibit some compaction and local ordering due to fragmentation and reaggregation. (c) Here $T = 1.04T_m$ and $t = 93\,905$. A higher degree of compaction is observed, and local ordering becomes more clear. Some of the clusters have begun to dissolve, as can be seen by the presence of monomers and smaller clusters. (d) Now $T = 1.05T_m$ and $t = 949\,489$. Fragmentation is highly pronounced here as can be seen by the proliferation of small clusters. The whole system is on the verge of dissolution.

of fragmentation and subsequent reaggregation. The branches of the clusters formed at this temperature are thicker than in the $T = T_m$ case. Even though fragmentation is allowed at this temperature, clusters are still large and extended with very few monomers or smaller clusters existing at late times. When the temperature is further increased to $T = 1.04T_m$, clusters become even more compact, and a local ordering among monomers becomes noticeable by visual inspection of the morphological images, indicating the beginning of crystallization. Bands of alternating-type particles are also noticeable. The presence of compact clusters in the system at this temperature is reflected in the increased value of the fractal dimension D_f as shown in Figure 3b, which climbs significantly past the final value for the irreversible, $T = T_m$, case (1.50−1.55) to a value above 1.60. However, at $T = 1.04T_m$, we also observe that very large clusters present at lower temperatures do not exist any longer. The system is composed instead of monomers, dimers, and a variety of other small clusters coexisting with some larger clusters. Finally, by $T = 1.05T_m$, fragmentation dominates at late times and does not allow large clusters to form. We have confirmed this by starting out with an initial configuration containing several very large clusters and then running the simulations for $T = 1.04$ and 1.05. In each case, the large clusters dissolved, leaving behind systems that were nearly identical to those formed from an initial configuration of monomers at those temperatures. From our studies, it is possible to estimate the dissolution temperature (T_{dis}) of the whole assembly. For the values of b_t and b_n considered here, $T_{dis} \approx 1.05T_m$.

(27) Pierce, F.; Chakrabarti, A.; Fry, D.; Sorensen, C. M. *Langmuir* **2004**, *20*, 2498−2502.
(28) Meakin, P.; Miyazima, S. *J. Phys. Soc. Jpn.* **1988**, *57*, 4439−4449.
(29) Family, F.; Meakin, P.; Vicsek, T. *J. Chem. Phys.* **1985**, *83*, 4144−4150.

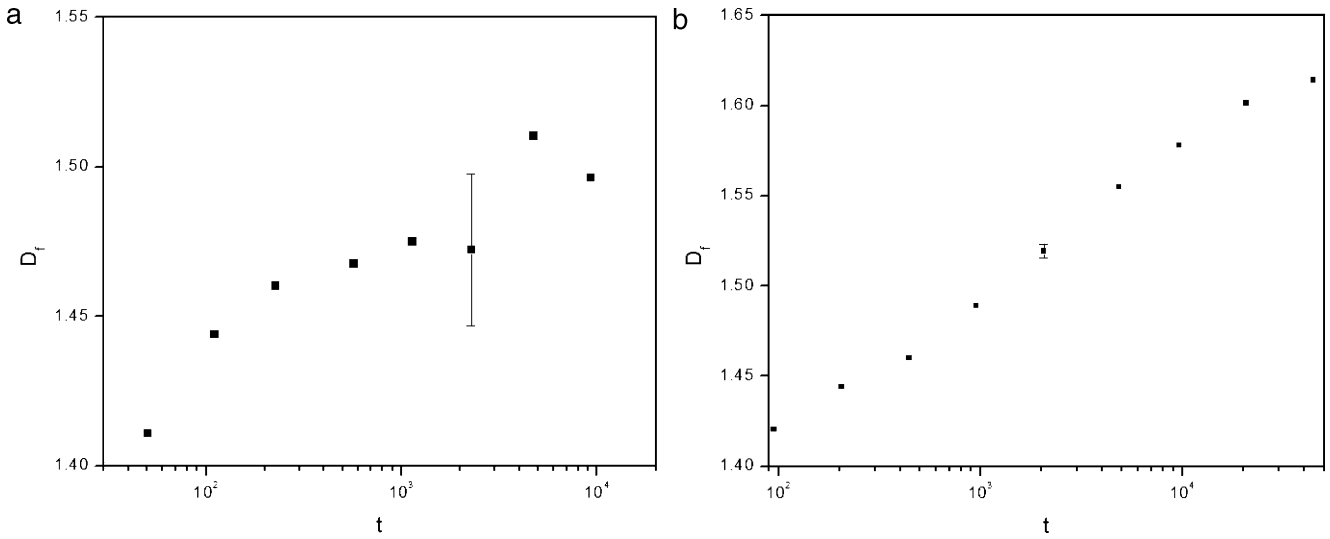

Figure 3. (a) Evolution of the fractal dimension D_f with time in the case of an overall area fraction of $f_a = 0.10$ with bonding configuration $b_t = 10$, $b_n = 3$ at the melting temperature T_m. The clusters begin to form with a fractal dimension close to that of the 2D DLCA value ($D_f = 1.4$) and evolve toward a higher value closer to the 2D RLCA value ($D_f = 1.55$). A characteristic error bar is shown. Error bars for other data points are of similar magnitude. (b) Same as in part a except $T = 1.04T_m$. The compaction of the clusters seen in Figure 2c is reflected in the increasing value of the fractal dimension D_f. It begins at a value close to the accepted 2D DLCA value of 1.4 and continues to rise past 1.6, indicating the formation of more compact clusters at late times. Beyond this temperature, steady-state clusters are too small for fractal dimension curves to have much meaning. A characteristic error bar is shown. Error bars for other data points are of similar magnitude.

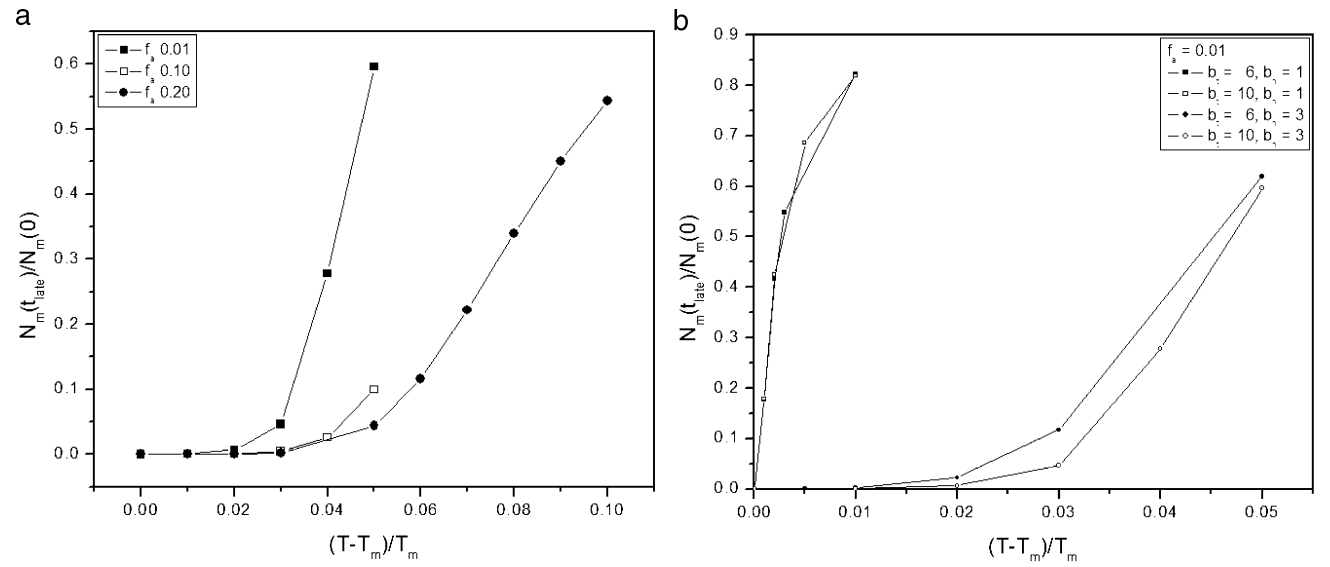

Figure 4. (a) Plot of the number of monomers left in the system at late times vs the scaled temperature $(T - T_m)/T_m$ for the bonding configuration $b_t = 10$, $b_n = 3$ for various area fractions. Notice the sharp temperature profiles. (b) Here we fix the area fraction at $f_a = 0.01$ and vary b_t and b_n. The dissolution temperature increases as one increases b_t. When $b_n = 1$, the value of b_t does not change the dissolution phase diagram appreciably. Even for $b_n > 1$, the effect of b_t on the dissolution phase diagram is still marginal.

In Figure 4a, we display a plot of the number of monomers left in the system at late times, $N_m(t_{late})$ versus the scaled temperature $(T-T_m)/T_m$ for the bonding configuration $b_t = 10$ and $b_n = 3$ at various area fractions. Because of computer time limitations, some of the simulations had not completely reached a steady state by the latest times available to us, as can be seen in the kinetics graphs (Figure 5a and b). In cases where the steady state cannot be reached within a reasonable amount of computer time, the temperature is close to the melting temperature, and the evolution process is dominated by aggregation. However in most of those cases, aggregation had nearly eliminated the presence of monomers in the system by the latest time, and further time evolution will be unlikely to alter $N_m(t_{late})$ significantly. Note that the temperature profile in Figure 4a is sharp in the case of area fraction $f_a = 0.01$ and becomes less sharp as the area fraction is increased. Such sharp dissolution temperature profiles are already seen in experiments. The decreased sharpness at higher area fractions perhaps originates from the stability of large clusters in an environment with a high degree of packing such as for $f_a = 0.10$ and 0.20. More bonds would have to be broken, on average, to dissociate a particle from its parent cluster in such cases, and the transition from a gellike phase to a dispersed, small-cluster phase becomes more gradual with temperature.

Similar random fractal and compact cluster morphology is observed at various temperatures for other values of b_t and b_n. As expected, the dissolution temperature depends on b_t and b_n. This is demonstrated in Figure 4b where we fix the area fraction to be $f_a = 0.01$ and vary b_t and b_n. The dissolution temperature increases as one increases b_t.

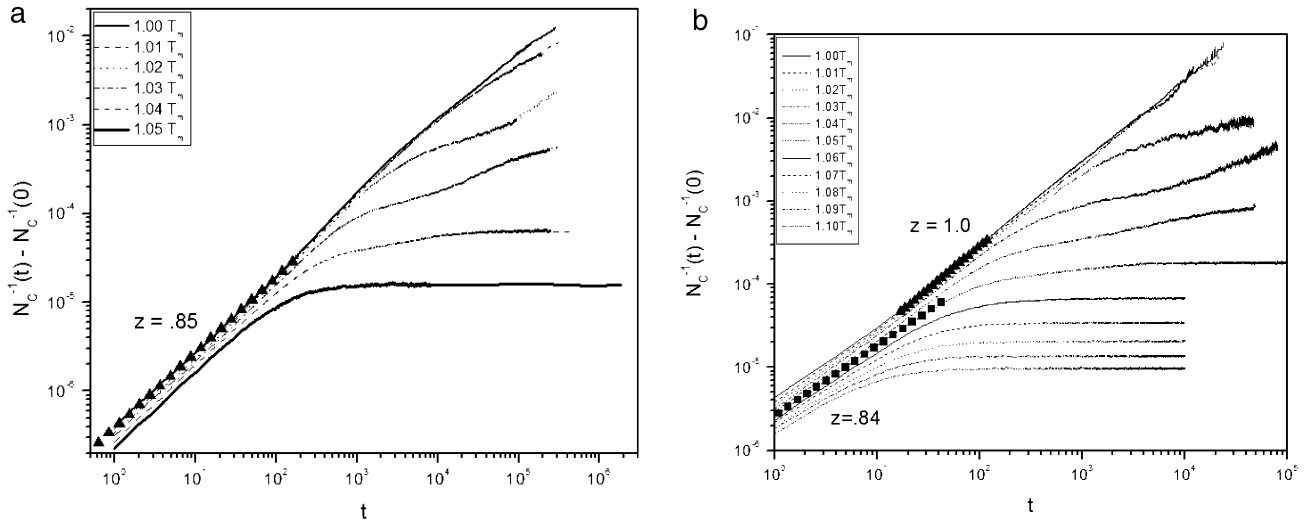

Figure 5. (a) Kinetics graph showing a log−log plot of inverse cluster number vs time (slope = z, the kinetic exponent) for the case of area fraction $f_a = 0.01$ and bonding configuration $b_t = 10$, $b_n = 3$ at various temperatures. As can be seen in the graph, all curves start with $z \approx 0.85$. As time progresses, the higher-temperature kinetics reach steady-state values, whereas the kinetic behavior is complicated at intermediate temperatures showing the appearance of inflection points. (b) Same as in part a but for area fraction $f_a = 0.10$. At lower temperatures, the early-time value of $z \approx 0.84$ increases to a higher value of $z \approx 1$ at intermediate times. This is consistent with the cluster crowding picture for 2D DLCA. Again, higher-temperature kinetics reach steady-state values, whereas the kinetic behavior is complicated at intermediate temperatures.

When $b_n = 1$, only one bond is allowed between each pair of A and B particles, and the dissolution temperature of the whole assembly (T_{dis}) is very close to the DNA melting temperature T_m. In this case, any single bond breaking splits a fractal cluster (of average coordination ~2) into two. One would expect then that the value of b_t would not change the dissolution phase diagram appreciably when $b_n = 1$. This is clearly demonstrated in Figure 4b. Even for $b_n > 1$, the effect of b_t on the dissolution phase diagram is still marginal. It is thus essential to have multiple DNA linking between each pair of A and B particles to have a large dissolution temperature. This result of our simulation agrees quite well with experimental observations.[16]

B. Kinetics of Growth. In Figure 5a and b, we show the inverse cluster number (N_c) versus time in a log−log plot for the $b_t = 10$, $b_n = 3$ bond configurations at monomer area fractions $f_a = 0.01$ and 0.10, respectively, with temperature T ranging from T_m to $1.05T_m$. For each area fraction f_a and temperature T, the early-time kinetic exponent $z \approx 0.85$ is consistent with 2D DLCA at these area fractions.[23] This indicates that at early times fragmentation does not play an important role in the cluster evolution process.

At $T = T_m$, the aggregation process is irreversible, and one might expect to see the same value of the kinetic exponent z throughout the evolution process. However, one needs to consider two different mechanisms that can change the kinetic exponent even in the irreversible case. First, it is known for the DLCA model that cluster crowding increases the kinetic exponent at late times. Second, as mentioned before, most collisions do not lead to the formation of aggregates at late times for the binary aggregation model studied here. This leads to a slowing of the late-time growth kinetics, particularly for smaller area fractions. The signature of such a slowing at late times is clear for $f_a = 0.01$ when $T = T_m$. For $f_a = 0.1$, z increases from 0.85 ± 0.03 to about 1.00 ± 0.02 at intermediate times before showing a hint of slowing down at late times. This increase in the kinetic exponent at intermediate times is consistent with the cluster crowding picture developed for the DLCA model.[30]

As the temperature is increased from T_m, fragmentation becomes important at late times, and the system should approach a steady state. This steady state is readily reached at higher temperatures, whereas it takes extremely long times for the system to reach the steady state near T_m. For temperatures near T_m such as for $T = 1.03T_m$, kinetic curves show the presence of inflection points, which are not observed in traditional aggregation−fragmentation models. To investigate the mechanism behind the inflection point, we focused on the behavior of the kinetic curves for $T = 1.03T_m$ by setting $f_a = 0.01$ and $b_n = 3$ but varying b_t from 3 to 10. These results are shown in Figure 6. The inflection points are not observed in the cases of $b_t < 8$. In addition, we notice that the higher the total number of bonds allowed per particle, the larger the final cluster size.

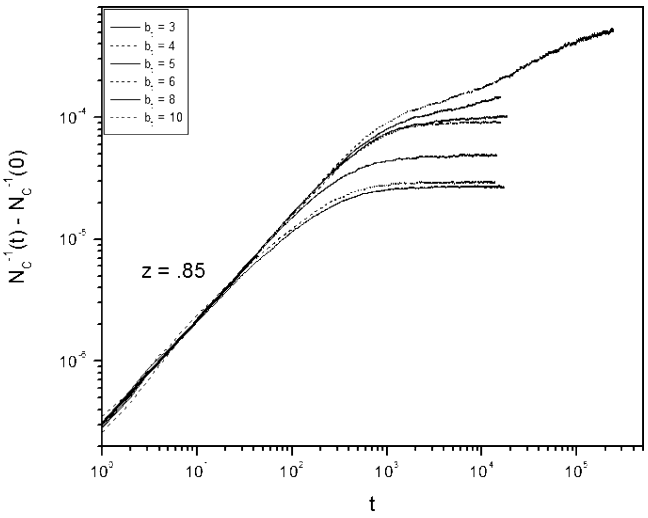

Figure 6. Kinetics curves for an overall area fraction of $f_a = 0.01$ and $b_n = 3$. Here b_t is varied from 3 to 10. For values of $b_t > 8$, inflections points can be seen in the kinetics graphs.

One possibility is that the inflection points are related to the geometry of the clusters as compaction takes place in stages during the aggregation process. To test this

(30) Fry, D.; Sintes, T.; Chakrabarti, A.; Sorensen, C. M. *Phys. Rev. Lett.* **2002**, *89*, 148301.

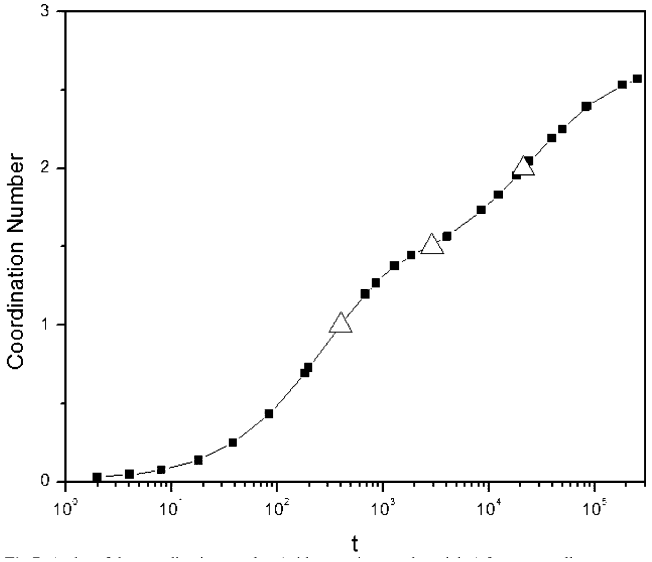

Figure 7. Plot of the coordination number (with opposite-typed particles) for an overall area fraction of $f_a = 0.01$ and bond configuration $b_t = 10$, $b_n = 3$ at an intermediate temperature of $1.03T_m$. Inflection points occur in similar positions to those seen in the kinetics data ($t = 400, 4000, 40\,000$) shown by the triangles.

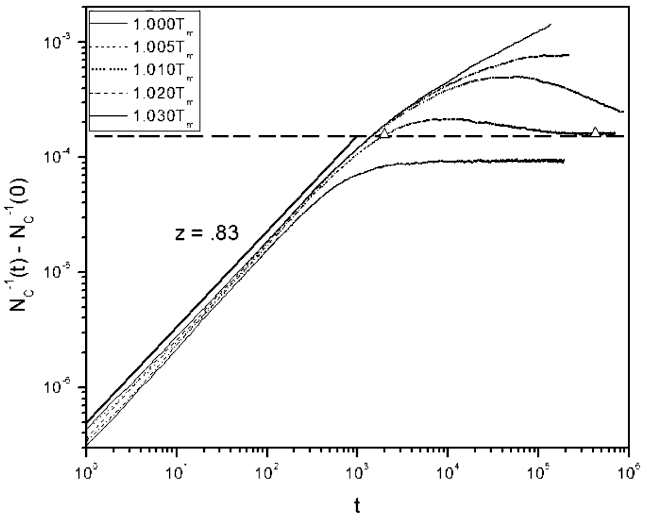

Figure 8. Kinetics curves for an overall area fraction of $f_a = 0.01$ with $b_t = 6$, $b_n = 3$. Here the temperature is varied from T_m to $1.03T_m$. The dashed horizontal line indicates the inverse cluster number corresponding to an average cluster size of four. The triangles represent two points on either side of the peak (at $t = 1977$ and 426 080, respectively) in the kinetics curve where the average cluster sizes in the system are similar to each other.

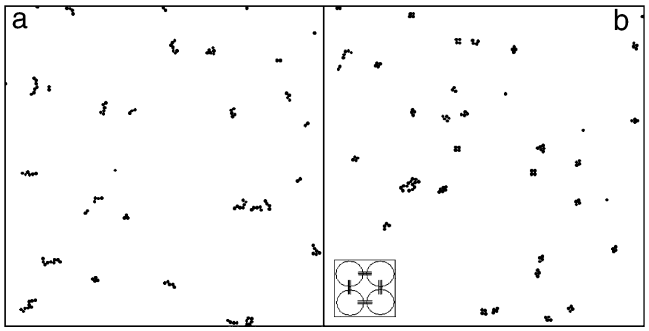

Figure 9. (a) Sample section of the system morphology for the case referred to in Figure 8 with $t = 1977$. The aggregates here are small but appear as the stringy precursors of DLCA-like aggregates. (b) Sample section of the system morphology for the case referred to in Figure 8 with $t = 426\,080$. The aggregates here are more compact than the previous case, and a proliferation of tetramers is apparent. The inset represents a possible stable bonding configuration (for $b_t = 6$, $b_n = 3$) leading to these four-particle clusters.

hypothesis, we plot in Figure 7 the time evolution of the average coordination number. We define the coordination number of a particle as the number of opposite-type neighbors it has within the cutoff distance of the bonding interaction. The coordination number exhibits similar inflection points previously observed in the kinetics graphs at roughly the same times (400, 4000, and 40 000 Monte Carlo steps). The average radius of gyration for clusters and the average nearest-neighbor distance also show similar inflection points indicating the geometric origin of the inflection points. The first inflection point occurs almost exactly where the average coordination number crosses the value of 1 and the third one near the value of 2. The coordination number seems to approach the steady-state value of three with time, corresponding to a tightly packed arrangement of particles. As a reference, we point out that the average coordination number of a system of dimers is 1 and that of large chains or DLCA-type clusters is 2. The average value of 3 indicates a structure that is more compact than normal DLCA-type fractal aggregates. This corroborates the cluster morphologies that we have observed at intermediate temperatures. Our results indicate that the inflections in the kinetic graphs are related to a geometric rearrangement of particle positions with time, where at certain stages of packing the average coordination number crosses integer (or possibly half integer) values, allowing more neighboring particles (of a different type) to fit next to a particular particle. At these times, the bonds available to a particular particle start to become shared among the now higher number of different types of neighbors, leading to the changes in the aggregation behavior.

Because the inflection points indicate a restructuring of the growing clusters to fit in more neighboring particles, they are sensitive to the values of b_t and b_n. In Figure 8, we show another set of cluster growth kinetics for $f_a = 0.01$ and for $b_t = 6$ and $b_n = 3$. The early-time growth exponent is consistent with previous results ($z \approx 0.83$), but now the growth kinetics is *not* monotonic at finite temperatures. We again suspect that this is due to the compaction of the clusters. To demonstrate this, we show snapshots of the cluster morphology for $T = 1.02$. We chose two times ($t = 1977$ and 426 080) placed around either side of the peak of the cluster size distribution such that the number of remaining clusters is approximately equal (denoted by two triangles on the graph). The horizontal line in Figure 8 represents the value of the inverse cluster number when the average cluster size is four monomers. In Figure 9a, we see a sampled section of the box showing the state of aggregation at $t = 1977$ with 4840 clusters remaining in the system. We observe that clusters, although small, have the somewhat stringy appearance of small DLCA-like aggregates. This is not altogether surprising because the kinetic growth curves for $T = T_m$ (pure aggregation case) and $T = 1.02T_m$ are not significantly different from each other at this time. However, by $t = 426\,080$, the above curves are noticeably different, and the appearance of the clusters for $T = 1.02T_m$ is significantly altered as can easily be seen in Figure 9b. Here the total number of clusters is very close to that of the previous time (4749), but the clusters are far more compact. In fact, the system seems to be dominated by tetramers. In the inset, a possible stable tetramer bonding

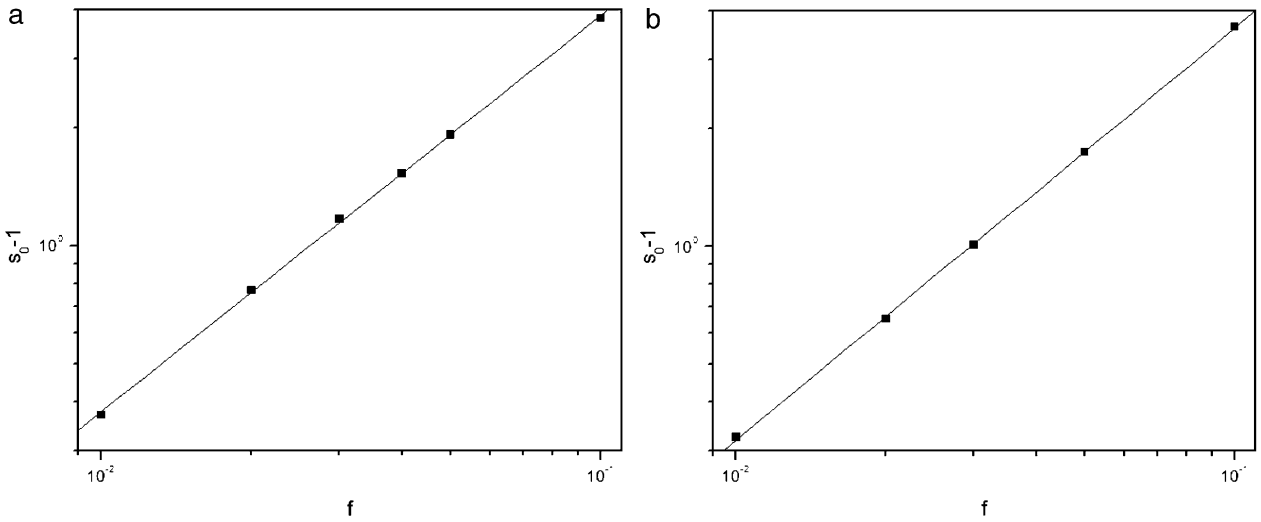

Figure 10. (a) log−log plot of the steady-state scaled value of the average cluster size vs overall area fraction in the case of $T = 1.003T_m$ with a bonding configuration of $b_t = 3$, $b_n = 1$. A best-fit line passes very near all data points, indicating the fact that scaling does work well in this case. The line has a slope of 1, yielding a fragmentation kernel exponent α of −1, assuming $\lambda = 0$ and $z = 1$. (b) Same as in part a except $T = 1.05T_m$ with a bonding configuration of $b_t = 10$, $b_n = 3$. The line has a slope of 1, yielding a fragmentation kernel exponent α of −1, assuming $\lambda = 0$ and $z = 1$.

configuration is shown in which particles have used all available bonds. This may explain why in the case of $b_t = 6$, $b_n = 3$ the system is driven toward these four-particle clusters at temperatures above the melting temperature. Of course, it may still be possible to develop larger stable aggregates at temperatures closer to the melting temperature. However, the amount of computer time needed to observe this would be enormous because some of our simulations have taken several weeks to reach completion, and possibly two more decades of time would be required to observe this effect.

C. Scaling Behavior at the Steady State. The steady-state value of the cluster size can be related to the homogeneity constants for aggregation (λ) and fragmentation (α). This is a result of the generalized Smoluchowski equation,[24,25] including both aggregation and fragmentation kernels K and F:

$$\frac{dn_k}{dt} = \frac{1}{2}\left[\sum_{i+j=k}(K(i,j)n_i n_j - F(i,j)n_{i+j})\right] - \left[\sum_{j=1}(K(k,j)n_k n_j - F(k,j)n_{k+j})\right]$$

The homogeneity exponents are expressed through the behavior of the aggregation and fragmentation kernels when the clusters aggregating from fragmentation are scaled in size by a factor of a:

$$K(ai, aj) = a^{\lambda}K(i,j) \text{ and } F(ai, aj) = a^{\alpha}F(i,j)$$

In addition, the kernels can be written in terms of an aggregation rate constant k_c and a fragmentation rate constant k_f in the following way

$$K(i,j) = k_c\Psi(i,j) \text{ and } F(i,j) = k_f\Phi(i,j)$$

where $\Psi(1, 1) = \Phi(1, 1) = 1$. Using the scaling equations, one then finds that the average cluster size s obeys the following differential equation

$$\frac{ds}{dt} = M_1 a k_c s^{\lambda} - b k_f s^{\alpha+2}$$

yielding a steady-state value s_0 for the average cluster size

$$s_0 = \left(\frac{M_1 a k_c}{b k_f}\right)^y$$

where y is a scaling exponent that can be written in terms of λ and α in the following way

$$y = (2 - \lambda + \alpha)^{-1}$$

Because M_1 represents the monomer area fraction f_a, one can compute the value of y by determining how the steady-state cluster size scales with the monomer area fraction. Because the value of the aggregation homogeneity constant λ is given by

$$\lambda = 1 - \frac{1}{z}$$

one can calculate α from the simulation, the fragmentation homogeneity constant. The value of α would be important to understanding how the fragmentations take place in the clusters.

One noteworthy point is that for higher temperatures in our simulation the steady-state average cluster size s_0 is not a very large number. Because s_0 evolves from a value of 1 (the system starts as a dispersion of monomers), it becomes important then to consider $s_0 - 1$ (instead of s_0) in our scaling analysis. Figure 10a and b portrays log−log plots of $s_0 - 1$ versus the area fraction f_a for two different sets of model parameters. Scaling seems to work quite well in each case, yielding $y = 1.0 \pm 0.05$. If we use the late-time (average cluster size >4) value of $z \approx 1$ for the kinetic exponent, we obtain $\alpha \approx -1$. These findings suggest that the fragmentation kernel decreases for larger clusters with a power law of exponent −1 for all of the bonding configurations and temperatures studied. This would indicate that larger clusters come apart more slowly than smaller clusters, leading to the interpretation that fragmentation is occurring at the surface of the clusters.

IV. Conclusions

We have carried out an off-lattice Monte Carlo simulation of DNA-mediated colloidal assembly where the aggregation−fragmentation of a binary mixture of colloidal

particles is studied through a simple model of base-pair hybridization between complementary DNA strands attached to the particles. A number of important insights can be obtained from these simulations. The morphologies of the aggregates we have observed are highly temperature-sensitive, varying from DLCA-like aggregates near the DNA melting temperature to aggregates with local ordering (and a hint of crystallization) at intermediate temperatures. Of course, to observe the details of such local crystal ordering a more robust model will be required, considering that such effects tend to be thermodynamic in nature and correspond to a minimization of the global free energy. Finally, the whole system dissolves into very small clusters at slightly higher temperatures. The sharpness of the temperature profiles seen in the morphologies is quantified by the number of unattached monomers left in the system at late times as a function of temperature. Simulation results agree with the experimental observation of sharp temperature profiles for DNA-mediated aggregation. The kinetics of growth shows an early time agreement with 2D DLCA results followed by a more complicated growth behavior. An increase in the kinetic exponent corresponding to cluster crowding at high area fractions is observed. Interestingly, we have also observed inflection points and a negative kinetic exponent under certain conditions, results attributed to the compaction of clusters above the melting temperature. This conclusion is supported by the increase in the mass fractal dimension with time as well as the evolution of the coordination number and its correspondence to the inflection points observed in the kinetics.

The presence of inflection points in the kinetics may represent a sort of punctuated equilibrium for this aggregation−fragmentation system, where aggregate bonding configurations stay relatively fixed for long periods of time but are separated by brief periods of bond restructuring. Of course this is not entirely surprising considering the geometrical constraints of spherical packing. Our cutoff length for the bonding of two opposite-type monomers is quite short, allowing bonding only at near contact for the monomer surfaces. The stringy DLCA aggregates of coordination number of 2 collapse as temperature exceeds the melting temperature because of the cyclic process of aggregation and fragmentation. This, of course, leads eventually to additional contacts between monomers as the aggregate structures seek free-energy minima. These new contacts then become available sites for bonding.

Finally, the steady-state behavior of the average cluster size indicates that over a wide range of bonding configurations the fragmentation of clusters happens at the surface.

Further study into these intriguing systems is certainly warranted because DNA-mediated colloidal aggregates can exhibit a wide variety of morphological forms, possibly leading to the development of new and diverse types of novel materials in addition to their potential use for the detection of small discrepancies in DNA coding.

Acknowledgment. Financial support from NASA under grant number NNC04GA74G is gratefully acknowledged.

LA050688Z